IOP Publishing Journal of Optics
J. Opt. 17 (2015) 105903 (6pp) doi:10.1088/2040-8978/17/10/105903

Enhancement of polycrystalline silicon solar cells efficiency using indium nitride particles

Sabri Alkis[1], Farsad Imtiaz Chowdhury[2], Mustafa Alevli[3], Nikolaus Dietz[4], Berna Yalızay[5], Selçuk Aktürk[5], Ammar Nayfeh[2] and Ali Kemal Okyay[6]

[1] Institute of Materials Science and Nanotechnology (UNAM), Bilkent University, Ankara, 06800, Turkey
[2] Institute Center for Future Energy Systems (iFES), Department of Electrical Engineering and Computer Science (EECS), Masdar Institute of Science and Technology, 54224, Abu Dhabi, United Arab Emirates
[3] Department of Physics, Marmara University, 34722, Istanbul, Turkey
[4] Department of Physics, Georgia State University, 3965, Atlanta, USA
[5] Physics Engineering Department, Istanbul Technical University, 34469, Istanbul, Turkey
[6] Department of Electrical and Electronics Engineering, Bilkent University, Ankara, 06800, Turkey

E-mail: sabrialkis@gmail.com

Received 25 May 2015, revised 22 June 2015
Accepted for publication 26 June 2015
Published 25 August 2015

Abstract

In this work, we present a hybrid indium nitride particle/polycrystalline silicon solar cell based on 230 nm size indium nitride particles (InN-Ps) obtained through laser ablation. The solar cell performance measurements indicate that there is an absolute 1.5% increase ($\Delta\eta$) in the overall solar cell efficiency due to the presence of InN-Ps. Within the spectral range 300–1100 nm, improvements of up to 8.26% are observed in the external quantum efficiency (EQE) and increases of up to 8.75% are observed in the internal quantum efficiency (IQE) values of the corresponding solar cell. The enhancement in power performance is due to the down-shifting properties of the InN-Ps. The electrical measurements are supplemented by TEM, Raman, UV/VIS and PL spectroscopy of the InN-Ps.

Keywords: particles, solar cell, enhancement, external quantum efficiency, internal quantum efficiency, efficiency, indium nitride

Introduction

The current capabilities of modern photovoltaic cells are being improved by the addition of semiconductor nanomaterials. Nowadays, efficient and promising photovoltaic cells are being built either based entirely on nanomaterials or by the combination of nanomaterials and the present bulk and thin film solar cell technology [1–5].

Recently performed studies have made significant achievements, not only in improving the conversion efficiencies, but also in expanding the spectral range of the existing photovoltaic cells using nanomaterials. Among these nanomaterials, semiconductor nanostructures act as effective components to improve the present photovoltaic cell performances [6–11]. Even though nanomaterial nonuniformity, and thin film and matrix inhomogeneity cause scattering and fluorescence loss within a photovoltaic cell, the performances of current photovoltaic cells could be improved by the fast luminescence properties of semiconductor nanomaterials due to their strong confinement effects [12–14]. Furthermore, thin films of semiconductor nanomaterials enable the separation and transport of excitons in the films and in addition, the light coupling efficiency and light penetration within the photovoltaic cells are improved [15]. Additionally, it is assumed that, upon being coupled with standard solar cell architectures, thin layers of semiconductor nanomaterials may also act as thin supportive antireflectance layers [15].

Due to these promising properties, various semiconductor nanomaterials such as CdSe quantum dots, ZnO nanostructures and silicon nanostructures have been explored in order to assess whether they can improve the efficiencies of current photovoltaic cells [7–9, 15]. Despite the above mentioned work leading to next generation nanomaterial enhanced photovoltaics, few reports have appeared in the literature regarding the use of semiconductor nanomaterials as efficiency enhancers for commercial polycrystalline silicon

solar cells [15, 16]. Nayfeh *et al* reported power improvements of 3–10% in the visible range upon the use of 1–3 nm size silicon nanoparticles as additive thin films in polycrystalline silicon solar cells [15].

Furthermore, Alkis *et al* reported the synthesis of indium nitride particles (InN-Ps) through laser ablation [17]. The near-infrared range photoluminescence properties of InN make this material advantageous in solar cell performance applications [23]. Intartaglia *et al* further proved that it is possible to obtain gram scale semiconductor particles through laser ablation, which is critical for large scale energy applications [18].

In this work, we demonstrate a particle/polycrystalline hybrid silicon solar cell that contains 230 nm size InN-Ps obtained through laser ablation of InN. Since the synthesis of InN-Ps requires toxic chemicals, its impact on environmentally friendly applications has to be assessed [15, 16]. In the following, the photovoltaic performance of InN-Ps enhanced solar cells is given, along with the materials and optical characteristics of laser synthesized InN-Ps.

Experimental details

InN-Ps in ethanol solution were obtained through the laser ablation of a high pressure chemical vapor deposition (HPCVD)-grown InN layer [19]. A Nd:glass femtosecond laser was used in the laser ablation process. The repetition rate was 1 kHz, the pulse duration was 550 fs and the pulse energy was 200 μJ. The beam was focused on the InN film target placed in ethanol, with a spherical lens of 200 mm focal distance. The fluence at the target was estimated to be around 3 J cm^{-2}. Under the laser illumination, the sample was raster-scanned at a rate of 1 mm s^{-1}. The overlap between many pulses on the sample surface yields complete film removal, thereby maximizing the overall particle density.

High resolution transmission electron microscopy (TEM) images of the InN-Ps were obtained using an FEI-Technai G^{2}F30 type instrument at an operating voltage of 300 kV. The Raman spectrum of the InN-Ps was obtained using a Witec Alpha 300 s micro Raman spectrometer with a Nb:YAG laser at an excitation wavelength of 532 nm. Silicon was used as the substrate. The optical absorption spectrum of the InN-Ps was obtained using a Varian Cary 5000 UV/Vis/NIR spectrometer and the photoluminescence spectrum was obtained using a Varian spectrofluorometer. The commercial polycrystalline solar cell has an area of 6.38 cm^2. It contains a thin silicon nitride infrared filtering antireflectance layer on top of an n-type silicon/p-type silicon polycrystalline junction that contains metallic grid lines for electrical contact measurements. The solar cell was obtained from the company top-solar_china. A photo of the solar cell is shown in figure 1.

InN-Ps were spin casted on top of this polycrystalline silicon junction multiple times, with a spin speed of 2000 rpm for 10 s in each step, and the solar cell's current voltage characteristics and spectral response were studied. For current–voltage characteristic study, the *J–V* curve testing system (Model IV5) of PV Measurement, Inc. was used. Before

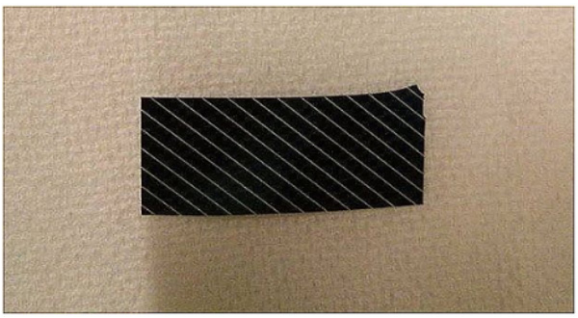

Figure 1. Photo of solar cell.

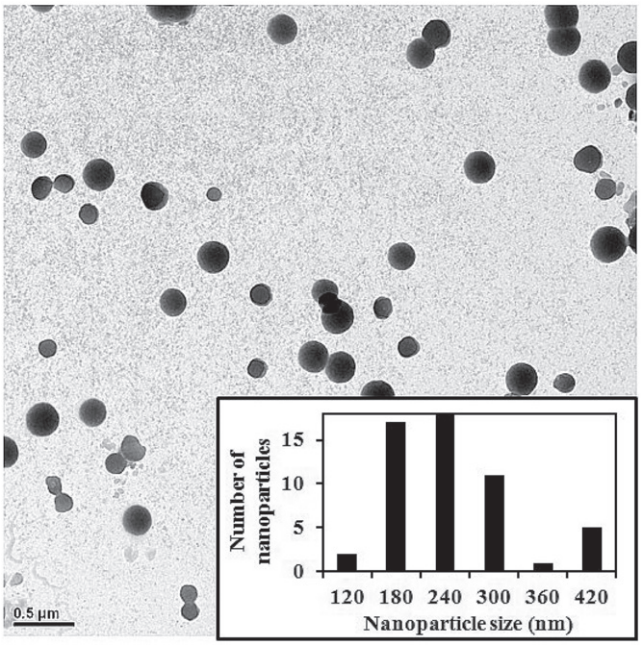

Figure 2. Transmission electron microscopy (TEM) image of laser synthesized InN-Ps with nanoparticle size distribution given in the inset.

measurement, the system was calibrated using a light meter to set the intensity of the light such that the irradiance equals one sun under AM1.5G. The spectral response of the fabricated device was measured using a solar cell spectral response measurement system (Model QEX7) from PV Measurement, Inc. Before measurement, this system was also calibrated using a silicon photodiode over the whole calibration range, between 300 nm and 1100 nm, at room temperature (23 $\pm$ 2 °C).

Results and discussion

The synthesized InN-Ps are spherical, without any aggregation and they have an average size of 230 nm as obtained from TEM images (depicted in figure 2) [20]. TEM results confirm the generation of InN-Ps through laser ablation.

The Raman spectrum of the InN-Ps is given in figure 3. The Raman spectrum shows Raman shift peaks at 480 cm^{-1} and 590 cm^{-1} representing the E_2(high) and A_1(LO) Raman

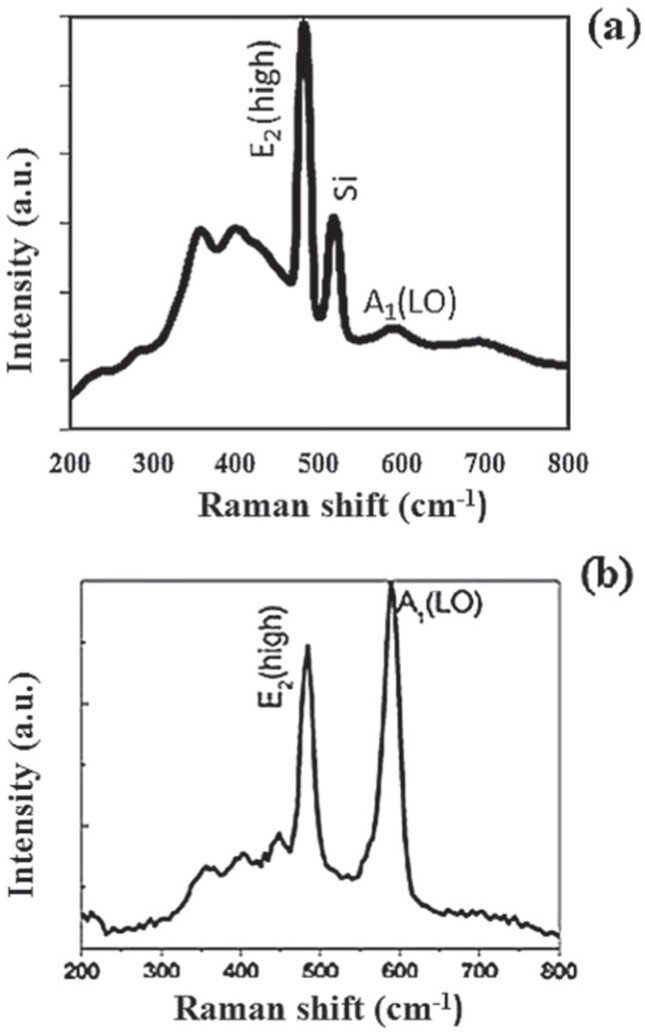

Figure 3. The Raman spectrum of InN-Ps dispersed on a silicon substrate (a), the Raman spectrum of InN thin film grown by HPCVD (b).

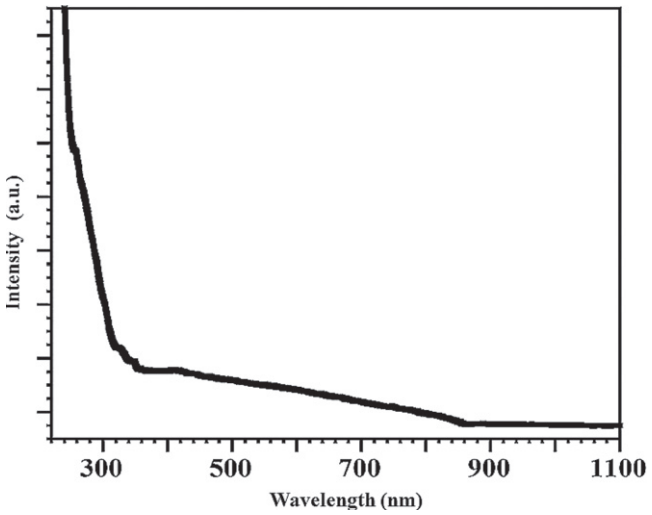

Figure 4. The UV–vis-NIR spectrum of InN-Ps.

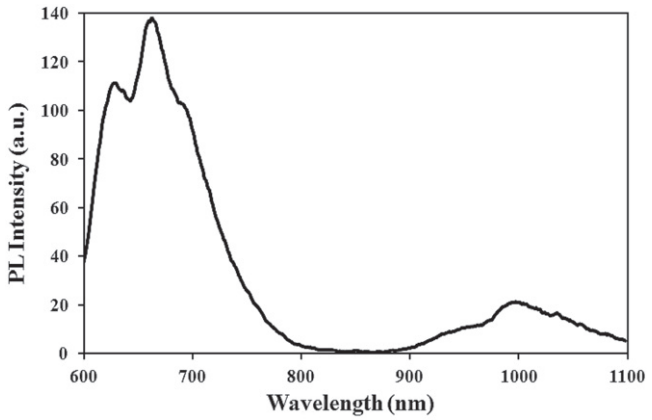

Figure 5. The PL spectrum of InN-Ps at an excitation wavelength of 300 nm at room temperature.

modes of InN, indicating that the InN-Ps have a hexagonal wurtzite structure (figure 3(a)) [17, 19]. In comparison with the InN thin film Raman spectrum, the observed deviations of the Raman peaks of the InN-Ps occur due to the formation of InN-Ps [17]. The full-width-at-half-maximum (FWHM) values of the E_2(high) phonon peaks indicate decent crystalline quality. The Raman results prove that the InN-Ps have good crystalline quality and therefore, we could conclude that the laser ablation process does not damage the material properties of the HPCVD-grown InN thin film [17, 19]. The Raman spectrum of the InN thin film obtained before the laser ablation is shown in figure 3(b).

The UV–vis-NIR absorption spectrum of the laser synthesized InN-Ps is given in figure 4. The UV–vis-NIR spectrum shows an absorption onset beginning at around 400 nm and minimum absorption features tailored down to 1100 nm due to the band gap of InN [17, 19]. The UV–vis-NIR spectrum of an InN thin film is given in the work of Alevli *et al* [19]. Differences between the two spectra are due to the formation of InN-Ps and the Moss–Burstein effect [17, 19, 21].

The photoluminescence spectrum of the InN-Ps at an excitation wavelength of 300 nm is given in figure 5. The PL spectrum shows a visible range luminescence peak at 666 nm that might arise from the indium cluster in the original films or from the effect of laser ablation, or it might also be a 'scattering' peak due to the light source [19, 22, 23]. The PL spectrum also consists of an **'NIR'** emission peak at around 1000 nm which dominates the spectrum, arising due to the band gap of InN [23]. Mainly, the shift from the band gap value of InN occurs due to the Moss–Burstein effect [21]. However, in a recent study performed by Alevli *et al* on InN thin films grown at different reactor pressures, they concluded that the variation in the band gap of InN films with free carrier concentrations above 10^{21} cm^{-3} does not vary due to the Moss–Burstein effect [24].

Figure 6 shows the *J–V* characteristics of the reference solar cell and the solar cell that contains InN-Ps under a voltage biasing condition of −1 V to 1 V. The *J–V* curve shows that there is a steady increase in *J* value down to the 0 V biasing condition, then the *J* value remains constant under 0 V to −1 V biasing conditions due to efficient collection of

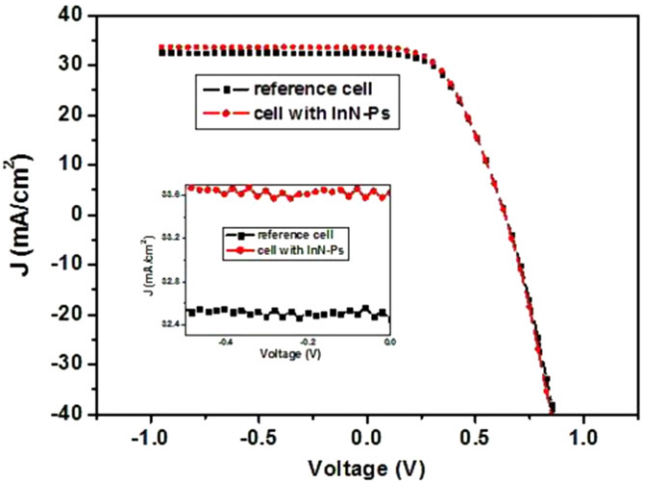

Figure 6. The *J–V* curve of the solar cells under a voltage biasing condition of 1 V to −1 V.

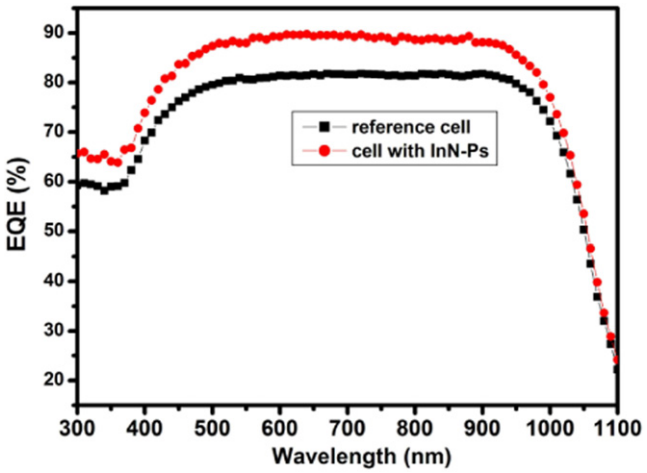

Figure 7. The external quantum efficiency of the reference solar cell and the cell that contains InN-Ps within the range 300–1100 nm.

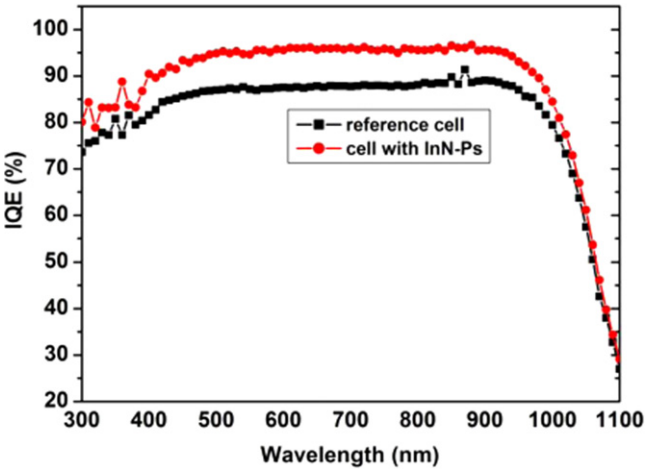

Figure 8. The internal quantum efficiency of the reference solar cell and the cell that contains InN-Ps, within the range 300–1100 nm.

charge carriers and the eventual saturation of the carrier drift velocities with the applied bias [25]. Under 0 V to −1 V biasing conditions, a current flux increase of 1 mA cm^{-2} is observed for the solar cell that contains InN-Ps.

Table 1 shows the results of the solar cell measurements, including the V_{oc} and J_{sc} values, efficiencies and fill factors obtained from the corresponding cells. The initial power conversion efficiency (η) of the solar cell that is used in this work is 12.5%. As seen from the table, a 0.68 mA cm^{-2} increase in the J_{sc} value leads to an absolute 1.5% increase ($\Delta\eta$) in the overall cell efficiency for the cell that contains InN-Ps.

In addition to solar cell measurements, figure 7 and figure 8 show the external and internal quantum efficiencies of the corresponding solar cells.

Figure 7 and figure 8 demonstrate that, under 300 nm light illumination, there is a 6.4% increase in EQE and a 6.5% increase in IQE for the cell that contains InN-Ps. The result of this increase could be explained by the visible and NIR absorption of the InN-Ps and the consequent down-shifting effect [17, 21, 27, 28]. Furthermore, for the cell that contains InN-Ps, a sharp increase is observed in the EQE and IQE values within the 300–500 nm range that could also be attributed to InN-Ps.

On the other hand, for both cells, the EQE and IQE values follow almost a linear trend within the 500–900 nm range with sharp falls in EQE and IQE values between 900 to 1100 nm due to the silicon band edge [25].

Moreover, by comparison of the EQE/IQE ratios for the reference cell and the cell that contains InN-Ps, an average improvement of 1% is observed in terms of the cell's ability to absorb sunlight within the 300–1100 nm range.

Figure 9 demonstrates the reflectivity values of the regular cell and the cell with InN-Ps within the 300–1100 nm range. It is seen that the reflectance of the solar cell decreases slightly between 300 and 400 nm which might be due to the down-shifting or due to the antireflectance properties of the InN-Ps. However, beyond 400 nm, no change is observed in the reflectivity curve, indicating that coating of the solar cell's surface with InN-Ps does not give a rise in antireflectance [28]. Therefore, we strongly believe that the increase in power performance efficiency of the solar cell is due to InN-Ps down-shifting properties [28].

Figure 10 demonstrates the ΔEQE and ΔIQE values within the 300–1100 nm wavelength range for the cell that contains InN-Ps.

Table 1. Solar cell efficiency parameters.

	V_{OC} (V)	J_{SC} (mA cm^{-2})	Efficiency (%)	Fill Factor
Reference Cell	0.62	34.38	12.50	59.04
Cell with InN-Ps	0.61	35.06	13.98	64.96

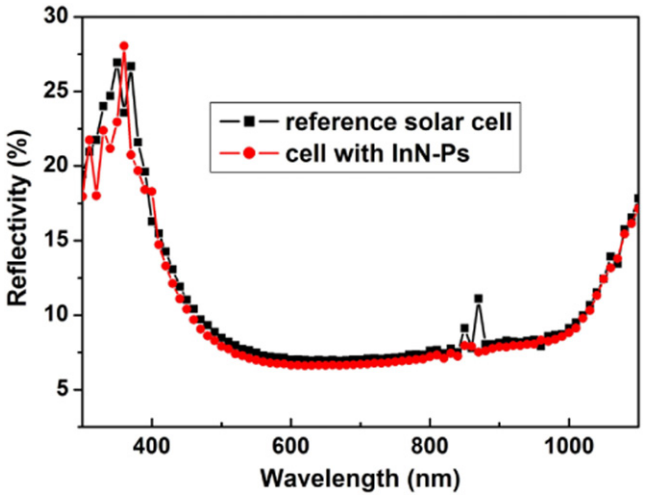

Figure 9. The reflectivity curve within the range 300–1100 nm.

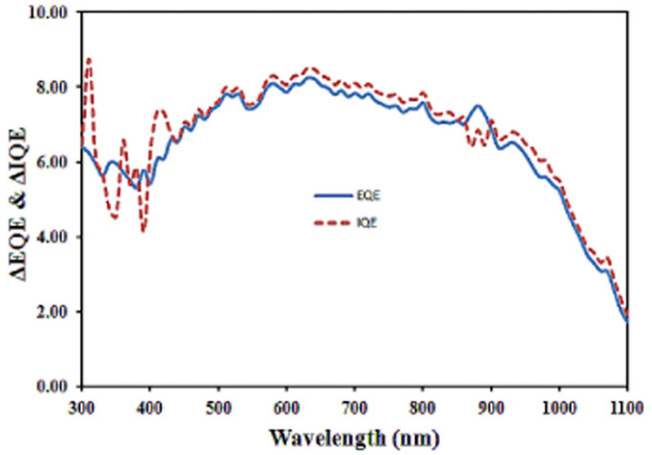

Figure 10. ΔEQE and ΔIQE values within the 300–1100 nm range for the cell that contains InN-Ps.

ΔEQE and ΔIQE values are obtained in comparison with the reference solar cell and they represent the percentage amount of quantum efficiency increment. According to figure 9, the ΔEQE and ΔIQE values are lower from 300 to 400 nm, compared to 400 to 600 nm. Peaks are observed around 600 nm and ΔEQE and ΔIQE values are observed to fall within the 600–1100 nm range, resembling the UV–vis-NIR spectrum of InN-Ps. However, the UV–vis-NIR absorption values of semiconductor particles shift due to the surrounding medium, which accounts for the difference between ΔEQE and ΔIQE, and the UV–vis-NIR absorption curves [26].

Conclusion

In this study, a proof of concept polycrystalline silicon solar cell that is spin coated with InN-Ps has been demonstrated. The absolute increase in efficiency ($\Delta\eta$) of the solar cell is observed to be 1.5% due to the presence of InN-Ps. InN-Ps' ability to enhance the efficiency of a commercial solar cell is confirmed by the EQE and IQE spectra. The observed enhancement in power performance is due to InN-Ps' down-shifting properties. Solar measurement results are supported by the materials and optical characteristics of the InN-Ps. The ability of laser ablation to provide good quality semiconductor particles in large quantities could lead to the fabrication of highly efficient and low cost photovoltaic cells that are of critical importance for today's energy industry.

Acknowledgments

This work was supported by the Scientific and Technological Research Council of Turkey (TUBITAK), Grant Nos. 109E044, 112M004, 112E052, and 113M815. A K Okyay acknowledges support from a European Union FP7 Marie Curie International Reintegration Grant (PIOS, Grant No. PIRG04-GA-2008-239444). A K Okyay acknowledges support from the Turkish Academy of Sciences Distinguished Young Scientist Award (TUBA GEBIP). We gratefully acknowledge Masdar Institute of Science and Technology for financial support.

References

[1] Akimov Y A, Koh W S, Sian S Y and Ren S 2010 *Appl. Phys. Lett.* **96** 073111
[2] Atwater H and Polman A 2010 *Nat. Mater.* **9** 205–13
[3] Chen X, Chen B, Jia B, Saha J K, Gai B, Stokes N, Qiao Q, Wang Y, Shi Z and Gu M 2012 *Nano Lett.* **12** 2187–92
[4] Kamat P V 2008 *J. Phys. Chem.* C **112** 1837
[5] Semonin O E, Luther J M, Choi S, Chen H-Y, Gao J, Nozik A J and Beard M C 2011 *Science* **334** 1530–3
[6] Islam K, Chowdhury F, Alnuami A and Nayfeh A 2014 *Photovoltaic Specialist Conf. (PVSC) IEEE 40th* 3071–5 (a)
[7] Yerokhov V Y and Melnyk I I 1999 *Renewable Sustainable Energy Rev.* **3** 291
[8] Martin-Palma R J, Vazques L, Martinez-Duart J M, Schnell M and Schaefer S 2001 *Semicond. Sci. Technol.* **16** 657
[9] Vrček V, Slaoui A and Muller J-C 2004 *Thin Solid Films* **384** 451–2
[10] Chowdhury F, Alnuami A, Islam K and Nayfeh A 2014 *Photovoltaic Specialist Conf, (PVSC) IEEE 40th* 2209–13
[11] Alkhatib A and Nayfeh A 2013 *Nat. Sci. Rep.* **3** 2099
[12] Allan G, Delerue C and Lannoo M 1996 *Phys. Rev. Lett.* **76** 2961
[13] Nayfeh O, Rao S, Smith A, Therrien J and Nayfeh M 2004 *IEEE Photonics Technol. Lett.* **16** 1927
[14] Nayfeh M H, Rao S, Nayfeh O, Amith A and Therrien J 2005 *IEEE Trans. Nanotechnol.* **4** 660
[15] Stupca M, Alsalhi M, Al Saud T, Almuhanna A and Nayfeh M H 2007 *Appl. Phys. Lett.* **91** 063107
[16] Chen J Y and Sun K W 2010 *Sol. Energy Mater. Sol. Cells* **94** 930–4
[17] Alkis S, Alevli M, Burzhuev S, Vural H A, Okyay A K and Ortaç B 2012 *J. Nanopart. Res.* **14** 1048
[18] Intartaglia R, Bagga K and Brandi F 2014 *Opt. Express* **22** 3117–27
[19] Alevli M, Atalay R, Durkaya G, Weesekara A, Perera A G U, Dietz N, Kirste R and Hoffmann A 2008 *J. Vacuum Sci. Technol.* A **26** 1023–6

[20] Kuzmin P G, Shafeev G A, Bukin V V, Garnov S V, Farcau C, Carles R, Warot-Fontrose B, Guieu V and Viau G 2010 *J. Phys. Chem.* C **114** 15266–73
[21] Tekcan B, Alkis S, Alevli M, Dietz N, Ortaç B, Biyikli N and Okyay A K 2014 *IEEE Electron Device Lett.* **35** 936–8
[22] Ivanov S V, Shubina T V, Jmerik V N, Vekshin V A, Kop'ev P S and Monemar B 2004 *J. Cryst. Growth* **269** 1–9
[23] Buegler M, Alevli M, Atalay R, Durkaya G, Senevirathna I, Jamil M, Ferguson I and Dietz N 2009 *Proc. SPIE* **7422** 742218
[24] Alevli M, Gungor N, Alkis S, Ozgit-Akgun C, Donmez I, Okyay A K, Gamage S, Senevirathna I, Dietz N and Biyikli N 2015 *Phys. Status Solidi* C **12** 423–9
[25] Alkis S, Tekcan B, Nayfeh A and Okyay A K 2013 *J. Opt.* **15** 105002
[26] Alkis S, Oruç F B, Ortaç B, Koşger A C and Okyay A K 2012 *J. Opt.* **14** 125001
[27] Pi X, Zhang L and Yang D 2012 *J. Phys. Chem.* C **116** 21240
[28] Pi X, Li Q, Li D and Yang D 2011 *Sol. Energy Mater. Sol. Cells* **95** 2941